

# Penta-Hepta Defect Chaos in a Model for Rotating Hexagonal Convection

Yuan-Nan Young and Hermann Riecke

*Department of Engineering Sciences and Applied Mathematics,  
Northwestern University, 2145 Sheridan Rd, Evanston, IL, 60208, USA*

(Dated: October 25, 2018)

In a model for rotating non-Boussinesq convection with mean flow we identify a regime of spatio-temporal chaos that is based on a hexagonal planform and is sustained by the *induced nucleation* of dislocations by penta-hepta defects. The probability distribution function for the number of defects deviates substantially from the usually observed Poisson-type distribution. It implies strong correlations between the defects in the form of density-dependent creation and annihilation rates of defects. We extract these rates from the distribution function and also directly from the defect dynamics.

PACS numbers: 47.20.Bp,47.54.+r,47.20.Ky,47.27.Te

Spatio-temporal chaos is at the focus of experimental [1, 2, 3, 4, 5, 6, 7, 8, 9] and of theoretical [10, 11, 12, 13, 14, 15] research in high-dimensional dynamical systems. Most of the extensive studies have been devoted to variants of thermally or electrically driven convection in thin liquid layers [3, 6, 7, 8, 11, 14]. Detailed experimental studies have also been performed on vertically vibrated layers of fluids [4] and on chemical systems [2]. Theoretically, various regimes of spatio-temporal chaos of the complex Ginzburg-Landau equation have been investigated [12, 16].

A striking feature of most spatio-temporally chaotic states are defects in the pattern. They can be line defects like domain walls, point defects like dislocations, disclinations, and spirals, or composite defects like penta-hepta defects. In particular dislocations have attracted great attention since they are easy to identify. Investigators have utilized their statistical, geometrical and dynamical aspects to quantify the chaotic states in which they arise. For example, the number of dislocations (spirals) in the wave patterns governed by the complex Ginzburg-Landau equation has been found to obey Poisson-type statistics [10]. This suggests the interpretation that in this system dislocations are created randomly in pairs with a fixed probability, after which they diffuse throughout the system without any mutual interaction until they annihilate each other in collisions [10]. The corresponding behavior and associated distribution function have also been found experimentally in electrically driven convection in nematic liquid crystals [1] and in thermally driven convection in an inclined layer [8], and theoretically in simulations of coupled Ginzburg-Landau equations for parametrically excited standing waves [15].

Geometric aspects of dislocations have been investigated in experiments on binary-mixture convection where the possibility to reconstruct the patterns from the dislocations has been explored [7]. In another study the geometry and connectivity of the dislocations' world lines in space-time has been considered [15]. Through the creation and annihilation events the world lines form loops in space-time. In studies of a type of defect-unbinding transition it has been found that the degree of order of

the defected pattern is related to the statistics of the size of the loops.

The dynamical relevance of dislocations has been suggested in direct simulations of the Navier-Stokes equations of spiral-defect chaos in Raleigh-Bénard convection. It was found that the chaotic state is by far most sensitive to perturbations during the creation of dislocation pairs [14]. The best evidence for the significance of defects as dynamical objects has been provided in simulations of the complex Ginzburg-Landau equation where the contribution of the defects to the Lyapunov dimension of the chaotic attractor has been extracted [13].

Most of the detailed analyses of spatio-temporal chaos and of its defects have been performed in disordered patterns that are based on stripes (or rolls). Much less work has been done on spatio-temporal chaos related to other planforms like rectangles [5] (and, related to it, vector waves [17]) or hexagons [2], and the role of the corresponding defects has been barely touched upon.

In this Letter we describe a spatio-temporally chaotic state that is based on a hexagonal pattern. Its disorder is closely tied in with the appearance of penta-hepta defects (PHDs), each of which consists of two dislocations in two of the three modes making up the hexagon pattern. In contrast to most other systems discussed above it is not only the instability of the background pattern that drives the chaotic state, but also the instability of the PHDs themselves. Thus, in the presence of PHDs new dislocations are created through *induced nucleation*. As a consequence the probability distribution function for the number of defects is considerably broader than the Poisson-type distributions reported in previous studies [1, 8, 10]. We obtain this persistent, chaotic state in a Swift-Hohenberg-type model for rotating non-Boussinesq convection at low Prandtl numbers. While induced nucleation itself has been reported previously [18, 19], without rotation it did not sustain persistent chaotic dynamics [18].

Motivated by the strong effect of mean flows and rotation on convection roll patterns [3, 6] we have previously studied their effect on the stability of hexagon patterns and their PHDs within the framework of Ginzburg-

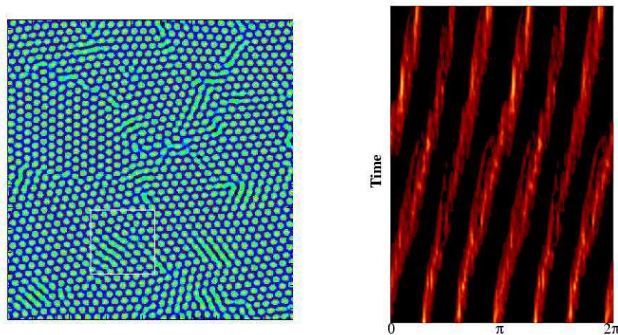


FIG. 1: a) Snapshot of penta-hepta defect chaos for  $\alpha = 0.4$ ,  $\gamma = 2$ ,  $\beta = -2.6$ ,  $R = 0.17$ , and  $L = 233$ . b) Corresponding space-time diagram of the radially integrated Fourier spectrum. A movie of the temporal evolution of the pattern and of its defects can be found on the EPAPS server.

Landau equations [19, 20]. Since the Ginzburg-Landau equations break the isotropy of the system they are not suited for investigations of spatio-temporal chaos. In this paper we therefore investigate a minimal extension of the Swift-Hohenberg model,

$$\begin{aligned} \partial_t \psi &= R\psi - (\nabla^2 + 1)^2 \psi - \psi^3 + \alpha (\nabla \psi)^2 + \gamma \hat{e}_z \cdot (\nabla \psi \times \nabla \Delta \psi) - \mathbf{U} \cdot \nabla \psi, \\ \nabla^2 \xi &= \hat{e}_z \cdot \nabla \Delta \psi \times \nabla \psi + \delta \{ (\Delta \psi)^2 + \nabla \psi \cdot \nabla \Delta \psi \}, \\ \mathbf{U} &= -\beta (\partial_y \xi, -\partial_x \xi). \end{aligned} \quad (1)$$

The quadratic terms proportional to  $\alpha$  and  $\gamma$  break the up-down symmetry  $\psi \rightarrow -\psi$  and model the non-Boussinesq effects. The chiral symmetry is broken by the terms involving  $\gamma$  and  $\delta$ ; thus, to leading order these coefficients are linear in the rotation rate. The mean-flow velocity and its stream function are given by  $\mathbf{U}$  and  $\xi$ , respectively, and  $\beta$  increases with decreasing Prandtl number. We simulate (1) numerically using a parallel pseudospectral code with periodic boundary conditions. A typical snapshot in the chaotic regime (Fig.1a) shows domains of hexagons of distinct orientations separated by domain walls in which many PHDs are aggregated. Due to the broken chiral symmetry most of the domains precess slowly counterclockwise. The corresponding space-time diagram for the temporal evolution of the radially integrated Fourier spectrum is presented in Fig.1b.

To identify the dislocations and PHDs we make use of the fact that despite the disorder of the pattern its spectrum exhibits six peaks that are clearly separated most of the time and that are rotated by  $120^\circ$  with respect to each other (cf. Fig.1b). We demodulate the pattern using three carrier wavevectors that slowly precess along with the spectrum,  $\psi = \sum_{j=1}^3 A_j \exp(i\mathbf{q}_j(t) \cdot \mathbf{r}) + h.o.t. + c.c..$  Figs.2a-c show the temporal evolution of a smaller section of the pattern with the dislocations in the three modes marked by triangles, squares, and circles, respectively. Open (closed) circles denote a positive (negative) topological charge of the dislocations.

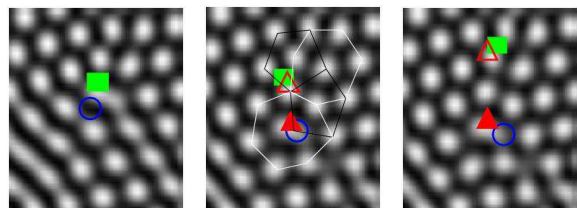


FIG. 2: Induced nucleation of dislocations. Enlargements corresponding to the box in Fig.1 at times  $t = 747$ ,  $t = 759$  and  $t = 760$ . Dislocations in  $A_i$ ,  $i = 1..3$ , marked by squares, circles, and triangles, respectively. Open (filled) symbols indicate positive (negative) topological charge. White (grey) lines mark heptagons (pentagons) making up the PHDs.

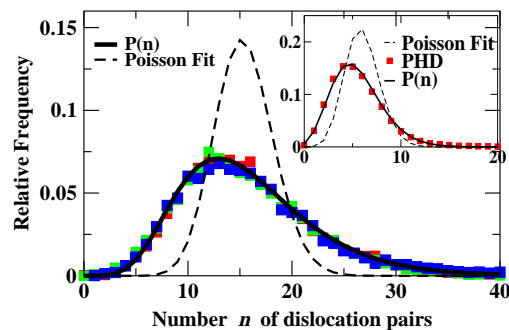


FIG. 3: Probability distribution function for the number of dislocation pairs in the pattern, the parameters are as in Fig.1 for  $L = 233$ . For the inset  $L = 114$ ,  $\alpha = 0.4$ ,  $\gamma = 3$ ,  $\beta = -5$  and  $R = 0.09$ . Solid line is fit to (4).

In various experimental and theoretical investigations of stripe-based disordered patterns the probability distribution function for the number of defects has been used to obtain a first characterization of the defect evolution [1, 8, 10]. Except for the ordered chaotic state in [15], the probability distribution function for the number of defects were found to be close to a Poisson-type distribution, indicating that the dynamics are consistent with the simple diffusive model described above with very weak correlations between the defects [10]. In particular, the creation rates depend only little on the defect density [8]. However, this is not the case for the defect chaos in hexagons. Fig.3 gives the distribution function for the number of dislocations in the penta-hepta defect chaos for two system sizes,  $L = 233$  and  $L = 114$  (inset), and two sets of parameter values. The symbols give the relative frequency to find  $n$  dislocation pairs in one of the three modes, whereas the dashed line gives the best fit to the squared Poisson distribution (with the same mean) corresponding to the uncorrelated dislocation dynamics [10]. Clearly, in the penta-hepta defect chaos the defect dynamics are far from uncorrelated.

A more detailed analysis of the defect dynamics reveals a strong tendency for dislocations to be created in

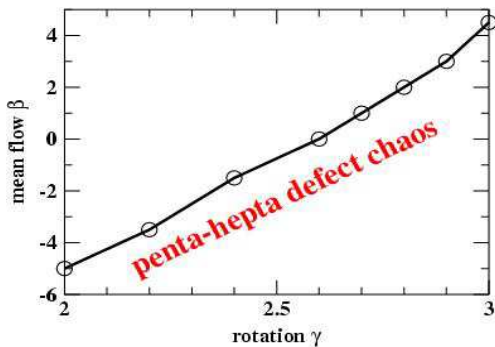


FIG. 4: Persistence limit for penta-hepta defect chaos as a function of  $\beta$  and  $\gamma$ . Other parameters as in inset of Fig.3 ( $L = 114$ ).

the vicinity of already existing PHDs. This is illustrated in Fig.2. Due to the gradient terms involving  $\alpha$  and  $\gamma$ , which lead to nonlinear gradient terms in the Ginzburg-Landau equations [21], the dislocations making up the PHDs are spatially separated [18, 19] (cf. Fig.2a). In addition, a PHD in modes  $A_1$  and  $A_2$ , say, leads to a perturbation in mode  $A_3$ . For sufficiently large  $\alpha$  and  $\gamma$  the perturbation evolves into a dislocation pair in mode  $A_3$  (in Fig.2b splitting of the cell between the ‘square’ and the ‘circle’ dislocation). The newly created dislocations then recombine with the oppositely charged dislocations in the original PHD to form two PHDs (Fig.2c), which then typically move apart from each other. Such *induced* defect nucleation has been found previously in coupled Ginzburg-Landau equations [18, 19] and in a Swift-Hohenberg-type model without rotation or mean flow [18]. However, in contrast to the case discussed in [18], in the presence of rotation the nucleation is sufficient to sustain a precessing chaotic state. As shown in Fig.4, for small Prandtl numbers ( $\beta < 0$ ) mean flow enhances the persistence of the chaotic state.

To establish a quantitative connection between the induced defect nucleation and the defect distribution function we consider an extension of the simple kinetic model for the dynamics of the defects presented in [10]. Since there are three different modes  $A_j$  and because the total topological charge of a PHD has to vanish [22], the statistics of the defect dynamics are described by a combined distribution function  $\mathcal{P}_6(n_{12}^+, n_{12}^-, n_{23}^+, n_{23}^-, n_{31}^+, n_{31}^-)$  for the six different kinds of PHDs. Here  $n_{12}^+$  denotes, for instance, the number of PHDs involving a dislocation with positive charge in mode  $A_1$  and a dislocation with negative charge in mode  $A_2$ . In principle, there are also dislocations that are not bound in a PHD. In this kinetic model we assume that their dynamics are fast enough to follow quickly the number of PHDs. The change in  $\mathcal{P}_6$  during a time interval  $\Delta t$  can be expressed in terms of creation and annihilation rates, which depend on the various defect densities. The numerical simulations show that the densities are strongly correlated at equal times [21], which implies that  $\mathcal{P}_6$  is strongly

peaked when its six arguments are equal. Integrating out the dependence of  $\mathcal{P}_6$  on five of its arguments, one therefore obtains a closed approximation for the change in  $\mathcal{P}(n_{12}^+ \equiv n) \equiv \int \mathcal{P}_6 dn_{12}^- dn_{23}^+ \dots dn_{31}^-$  during a time interval  $\Delta t$  involving the creation and annihilation rates  $\Gamma_n^\pm$ ,

$$\mathcal{P}(t + \Delta t, n) = \mathcal{P}(t, n) + \Delta t \{ \Gamma_{n-1}^+ \mathcal{P}(t, n-1) + \Gamma_{n+1}^- \mathcal{P}(t, n+1) - (\Gamma_n^- + \Gamma_n^+) \mathcal{P}(t, n) \}. \quad (2)$$

In steady state the distribution function satisfies detailed balance,  $\mathcal{P}(n+1) \Gamma_{n+1}^- = \mathcal{P}(n) \Gamma_n^+$ . Assuming a fixed rate for the induced nucleation, the rate for the process shown in Fig.2 depends linearly on the density of the ‘square-circle’ PHDs. It creates one ‘triangle-circle’ (and one ‘triangle-square’) PHD and annihilates the original ‘square-circle’ PHD. This suggests a linear contribution to the dependence of the annihilation and creation rates on the defect density. The reverse process originates from two PHD’s and therefore contributes quadratic terms. Including also the spontaneous creation of dislocations, which then form PHDs, we make the ansatz

$$\Gamma_n^- = a_1 n + a_2 n^2, \quad \Gamma_n^+ = c_0 + c_1 n + c_2 n^2. \quad (3)$$

Since the probability distribution depends only on the relative rates we choose the overall time scale to normalize the coefficient  $a_2$  of the quadratic annihilation rate to unity. The steady-state solution to (2,3) is then given by

$$\mathcal{P}(n) = \mathcal{P}(0) \prod_{j=0}^{n-1} \frac{c_0 + c_1 j + c_2 j^2}{a_1 (j+1) + (j+1)^2}, \quad (4)$$

with  $\mathcal{P}(0)$  determined by the normalization condition. A fit of the numerical simulation results to (4) is shown as solid line in Fig.3 and its inset. For both system sizes the fits are very good. For  $L = 114$  we obtain  $c_0 = 20.7$ ,  $c_1 = 20.7$ ,  $c_2 = 0.12$ , and  $a_1 = 8.6$  ( $a_2$  is scaled to unity), confirming the strong dependence of the creation rate on the number of defects.

By tracking each dislocation from its creation to its annihilation we can also determine the creation and annihilation rates directly from the numerical simulations. Fig.5 shows these rates for a dislocation in a given mode as a function of the number of dislocation pairs in the same mode for a system of size  $L = 114$  (same parameters as in inset of Fig.3). In principle, the rates should be given as functions of the number of PHDs involving the other modes. However, due to the finite distance between the dislocations within a PHD the grouping of dislocations into PHDs is not always unique. Because the numbers of dislocations in the three modes are strongly correlated, taking the number of dislocations in the same mode provides a good approximation. The large scatter in the data for larger defect numbers is due to the lack of statistics for events of that kind (cf. inset of Fig.3). Similarly, there are only few events with few defects. Clearly, in the intermediate range of  $n$  not only the annihilation

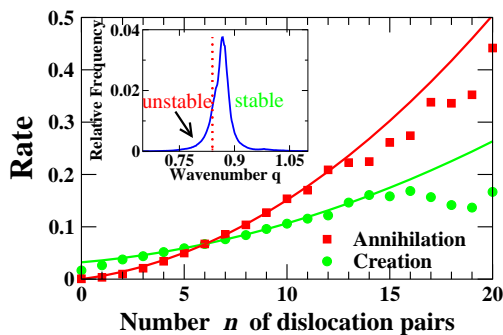


FIG. 5: Creation (squares) and annihilation (circles) rates of dislocations as a function of the number of dislocation pairs in the same mode. Parameters as in inset of Fig.3 ( $L = 114$ ). Inset: wavenumber distribution function with stability limit for hexagons according to weakly nonlinear theory (dashed).

rate but also the creation rate depends strongly on the defect number.

To connect the directly measured rates with the distribution function (4) the solid curves in Fig.5 give the creation and annihilation rates as determined from fitting the distribution function for the defect number using the form (3). For this comparison the overall time scale is adjusted to fit the time scale of the simulations. Clearly, the rates inferred from Fig.3 agree quite well with the directly measured ones over the statistically reliable range of  $n$  and confirm the interpretation of the deviation of the distribution function from the squared Poisson distribution.

The creation rate for dislocations does not vanish for  $n = 0$ , i.e. when no PHDs are present. This indicates the spontaneous creation of dislocation pairs directly from an instability of the hexagonal pattern, although the mean wavenumber of the background pattern is clearly inside

the stability balloon. However, the distribution function for the local wavenumber (inset of Fig.5) shows that there is a noticeable tail of the distribution function that extends beyond the low- $q$  stability limit, as determined by a weakly nonlinear analysis of (1). This suggests that some dislocation pairs are created through a side-band instability of the periodic pattern.

In conclusion, in a model for rotating non-Boussinesq convection we have identified a spatio-temporally chaotic state that is dominated by the dynamics of penta-hepta defects of the underlying hexagon pattern. In contrast to previously analyzed chaotic states, which are stripe-based, the defect statistics of this penta-hepta chaos indicate strong correlations between the defects. We identify the origin of the correlations as the induced nucleation of dislocations due to the presence of penta-hepta defects. From the defect statistics we extract the dependence of the creation and annihilation rates of defects on the defect density and find good agreement with the rates measured directly by following individual defects in the simulations. In ongoing direct simulations of the Navier-Stokes equations for rotating non-Boussinesq convection we have identified regimes exhibiting induced nucleation of dislocations [23]. In the simulations performed so far the induced nucleation either occurs only as a transient and eventually leads to ordered hexagon patterns or it leads to persistent chaotic dynamics that are somewhat more complex than the dynamics found here for the extended Swift-Hohenberg model.

We wish to acknowledge useful discussion with A. Golovin, A. Nepomnyashchy, and L. Tsimring. This work was supported by grants from the Department of Energy (DE-FG02-92ER14303), NASA (NAG3-2113), and NSF (DMS-9804673). YY acknowledges computation support from the Argonne National Labs and the DOE-funded ASCI/FLASH Center at the University of Chicago.

- 
- [1] I. Rehberg, S. Rasenat, and V. Steinberg, Phys. Rev. Lett. **62**, 756 (1989).
  - [2] Q. Ouyang and H. Swinney, Chaos **1**, 411 (1991).
  - [3] S. Morris, E. Bodenschatz, D. Cannell, and G. Ahlers, Phys. Rev. Lett. **71**, 2026 (1993).
  - [4] A. Kudrolli and J. Gollub, Physica D **97**, 133 (1996).
  - [5] M. Dennin, G. Ahlers, and D. S. Cannell, Science **272**, 388 (1996).
  - [6] Y. Hu, W. Pesch, G. Ahlers, and R. E. Ecke, Phys. Rev. E **58**, 5821 (1998).
  - [7] A. La Porta and C. M. Surko, Physica D **139**, 177 (2000).
  - [8] K. E. Daniels and E. Bodenschatz, Phys. Rev. Lett. **88**, 034501 (2002).
  - [9] E. Bodenschatz, W. Pesch, and G. Ahlers, Ann. Rev. Fluid Mech. **32**, 709 (2000).
  - [10] L. Gil, J. Lega, and J. Meunier, Phys. Rev. A **41**, 1138 (1990).
  - [11] W. Decker, W. Pesch, and A. Weber, Phys. Rev. Lett. **73**, 648 (1994).
  - [12] H. Chaté and P. Manneville, Physica A **224**, 348 (1996).
  - [13] D. A. Egolf, Phys. Rev. Lett. **81**, 4120 (1998).
  - [14] D. A. Egolf, I. V. Melnikov, W. Pesch, and R. E. Ecke, Nature **404**, 733 (2000).
  - [15] G. D. Granzow and H. Riecke, Phys. Rev. Lett. **87**, 174502 (2001).
  - [16] I. S. Aranson and L. Kramer, Rev. Mod. Phys. **74**, 99 (2002).
  - [17] E. Hernández-García, M. Hoyuelos, P. Colet, and M. S. Miguel, Phys. Rev. Lett. **85**, 744 (2000).
  - [18] P. Colinet, A. A. Nepomnyashchy, and J. C. Legros, Europhys. Lett. **57**, 480 (2002).
  - [19] Y.-N. Young and H. Riecke, Physica D (submitted).
  - [20] Y.-N. Young and H. Riecke, Physica D **163**, 166 (2002).
  - [21] Y.-N. Young and H. Riecke, in preparation (2003).
  - [22] M. Rabinovich and L. Tsimring, Phys. Rev. E **49**, 35 (1994).
  - [23] Y.-N. Young, H. Riecke, W. Pesch, and V. Moroz, (unpublished).